Premature termination codons in the DMD gene cause reduced local mRNA synthesis

Garcia-Rodriguez, R.; Hiller, M.; Jimenez-Gracia, L.; Pal, Z. van der; Balog, J.; Adamzek, K.; ... ; Spitali, P.

Premature termination codons in the *DMD* gene cause reduced local mRNA synthesis

Raquel García-Rodríguez[a,1], Monika Hiller[a,1], Laura Jiménez-Gracia[a,1], Zarah van der Pal[a], Judit Balog[a], Kevin Adamzek[a], Annemieke Aartsma-Rus[a], and Pietro Spitali[a,2]

[a]Department of Human Genetics, Leiden University Medical Center, 2333ZA Leiden, The Netherlands

Edited by Louis M. Kunkel, Boston Children's Hospital, Harvard Medical School, Boston, MA, and approved June 2, 2020 (received for review June 19, 2019)

Duchenne muscular dystrophy (DMD) is caused by mutations in the *DMD* gene leading to the presence of premature termination codons (PTC). Previous transcriptional studies have shown reduced DMD transcript levels in DMD patient and animal model muscles when PTC are present. Nonsense-mediated decay (NMD) has been suggested to be responsible for the observed reduction, but there is no experimental evidence supporting this claim. In this study, we aimed to investigate the mechanism responsible for the drop in *DMD* expression levels in the presence of PTC. We observed that the inhibition of NMD does not normalize *DMD* gene expression in DMD. Additionally, in situ hybridization showed that DMD messenger RNA primarily localizes in the nuclear compartment, confirming that a cytoplasmic mechanism like NMD indeed cannot be responsible for the observed reduction. Sequencing of nascent RNA to explore *DMD* transcription dynamics revealed a lower rate of *DMD* transcription in patient-derived myotubes compared to healthy controls, suggesting a transcriptional mechanism involved in reduced DMD transcript levels. Chromatin immunoprecipitation in muscle showed increased levels of the repressive histone mark H3K9me3 in *mdx* mice compared to wild-type mice, indicating a chromatin conformation less prone to transcription in *mdx* mice. In line with this finding, treatment with the histone deacetylase inhibitor givinostat caused a significant increase in DMD transcript expression in *mdx* mice. Overall, our findings show that transcription dynamics across the *DMD* locus are affected by the presence of PTC, hinting at a possible epigenetic mechanism responsible for this process.

Duchenne muscular dystrophy | premature termination codons | nascent RNA | RNA degradation | skeletal muscle

Duchenne muscular dystrophy (DMD) is a rare genetic disorder caused by mutations in the *DMD* gene resulting in premature termination codons (PTC) and, therefore, the absence of functional dystrophin protein. Lack of dystrophin is responsible for instability of skeletal muscle fibers and cardiomyocytes during contraction, leading to continuous muscle damage and weakness (1). Multiple drug developers focused on the identification of compounds able to correct the mutation at the posttranscriptional level by, for example, exon skipping (2, 3) or stop codon read-through (4). While these approaches have shown positive results in preclinical models (5–7) and DMD patients (2, 8), their success is limited by multiple factors such as inefficient delivery to muscle tissue, but also reduced levels of their drug target, namely, the dystrophin transcript. Indeed, transcriptional studies have shown that dystrophin messenger RNA (mRNA) levels are heavily reduced in muscle when premature stop codons are present (9, 10). The field has assumed that reduced transcript levels are caused by nonsense-mediated decay (NMD) (11–14), which is the cytoplasmic surveillance mechanism in charge of the mRNA quality control before translation (15). During the first round of translation, mRNAs are controlled for the presence of premature stop codons and degraded, should their presence be detected. While it is plausible that dystrophin mRNA levels are reduced due to NMD, there is no experimental evidence supporting this claim. Given the presence of dystrophin mRNA transcripts in muscle despite the presence of PTC, it has been proposed, in the literature, that NMD may be somewhat less efficient for dystrophin mRNA (16). Furthermore, reduced transcript levels have been observed in patients affected by Becker muscular dystrophy (BMD) (17), which is the milder allelic form of the disease caused by in-frame mutations and where, therefore, premature stop codons are not present. Yet, levels of dystrophin mRNA have been shown to be reduced, especially toward the 3′ end as for DMD- and BMD-causing mutations (18, 19). In fact, reduced transcript accumulation toward the 3′ end has also been observed in healthy controls (HCs) (20), suggesting that transcription of the locus is challenging, which is not surprising given that the *DMD* gene is one of the largest genes in the human genome, spanning 2.2 Mb.

With this work, we aimed to study how the presence of PTC affects dystrophin mRNA levels in muscle and to clarify which mechanism is responsible for reduced transcript amounts in the presence of dystrophin-truncating mutations.

Results

We studied *Dmd* gene expression in both skeletal and cardiac muscles of *mdx* mice carrying a nonsense mutation in exon 23 of the mouse *Dmd* gene. RNA sequencing (RNA-seq) data

Significance

Duchenne muscular dystrophy is a rare disease caused by lack of dystrophin due to mutations in the *DMD* gene. The presence of mutations leads to a reduction of the transcript levels. In this study, we show that the transcript reduction is not caused by the cytoplasmic nonsense-mediated decay mechanism as previously thought. We demonstrate that dystrophin mRNA is primarily localized in the nuclear compartment of skeletal muscle fibers. Analysis of nascent RNA and histone marks shows that transcription is less efficient in the presence of premature termination codons. Treatment of dystrophic mice with an epigenetic drug, currently in clinical development, partially restores transcription of the locus. This work will help the development of RNA targeting therapies for Duchenne patients.

Author contributions: P.S. designed research; R.G.-R., M.H., L.J.-G., Z.v.d.P., and K.A. performed research; J.B., A.A.-R., and P.S. contributed new reagents/analytic tools; R.G.-R., Z.v.d.P., and P.S. analyzed data; R.G.-R. and P.S. wrote the paper; and A.A.-R. and P.S. supervised the project.

The authors declare no competing interest.

This article is a PNAS Direct Submission.

Data deposition: RNA-seq data have been uploaded on Gene Expression Omnibus, and they are available at https://www.ncbi.nlm.nih.gov/geo/query/acc.cgi?acc=GSE132741. Bru-seq data is available at https://www.ncbi.nlm.nih.gov/geo/query/acc.cgi?acc=GSE153453.

[1]R.G.-R., M.H., and L.J.-G. contributed equally to this work.

[2]To whom correspondence may be addressed. Email: P.Spitali@lumc.nl.

This article contains supporting information online at https://www.pnas.org/lookup/suppl/doi:10.1073/pnas.1910456117/-/DCSupplemental.

First published July 2, 2020.

obtained from the tibialis anterior muscle showed that the Dmd transcript is the most significantly down-regulated gene in *mdx* muscle (adjusted $P < 10^{-97}$), with a fourfold reduction compared to wild-type (wt) mice (Fig. 1 *A*–*C*). The qPCR confirmed the down-regulation in cardiac muscle at different ages ranging from 2- to 10-mo-old mice. The qPCR data clarified that the transcript levels were particularly reduced toward the 3′ end compared to the wt counterpart (Fig. 1*D*). To assess whether the reduction is specific for the Dmd transcript or a consequence of the dystrophic pathological pathways, we analyzed the Htt transcript, which has a comparable transcript size (13 kb). A reduction toward the 3′ end of the Htt transcript was not visible in *mdx* mice (Fig. 1*E*).

To evaluate whether the transcript reduction is caused by NMD, we treated control and DMD-derived (deletion of exons 48 to 50) myotubes with cycloheximide (CHX), a compound known to block translation and NMD. Absolute transcript quantification by droplet digital PCR (ddPCR) showed reduced DMD transcript levels in DMD cells compared to HCs, especially toward the 3′ end (Fig. 2 *A*, *Left*). This observation suggests that reduced transcript levels are not species or mutation specific but are due to the presence of PTC (nonsense mutation in exon 23 in *mdx* mice and deletion of exons 48 to 50 in human DMD cells). After CHX treatment, an average increase of ∼1,500 copies per μL was observed in treated cells compared to untreated ones ($P < 10^{-14}$), suggesting that the DMD mRNA is subjected to NMD in both HC and DMD cells. The increase following treatment with CHX was comparable across DMD and HC cells, suggesting that NMD is not specifically more active on the DMD mRNA in the presence of PTC. Reduced transcript accumulation at the 3′ end in DMD-derived cells was not normalized by treatment (Fig. 2 *A*, *Right*).

Additionally, to assess whether NMD blockade corrects *DMD* expression when a different *DMD* mutation is present, we transfected primary DMD-derived (point mutation in exon 6 of the *DMD* gene) myotubes with a small interfering RNA (siRNA) targeting UPF1 [NMD master regulator (21)], along with a control siRNA. After 72 h of transfection, siRNA-mediated down-regulation of UPF1 showed ∼60% knockdown of the target gene (Fig. 2*B*). However, the knockdown was not able to correct the reduced accumulation of the 3′ end, supporting that

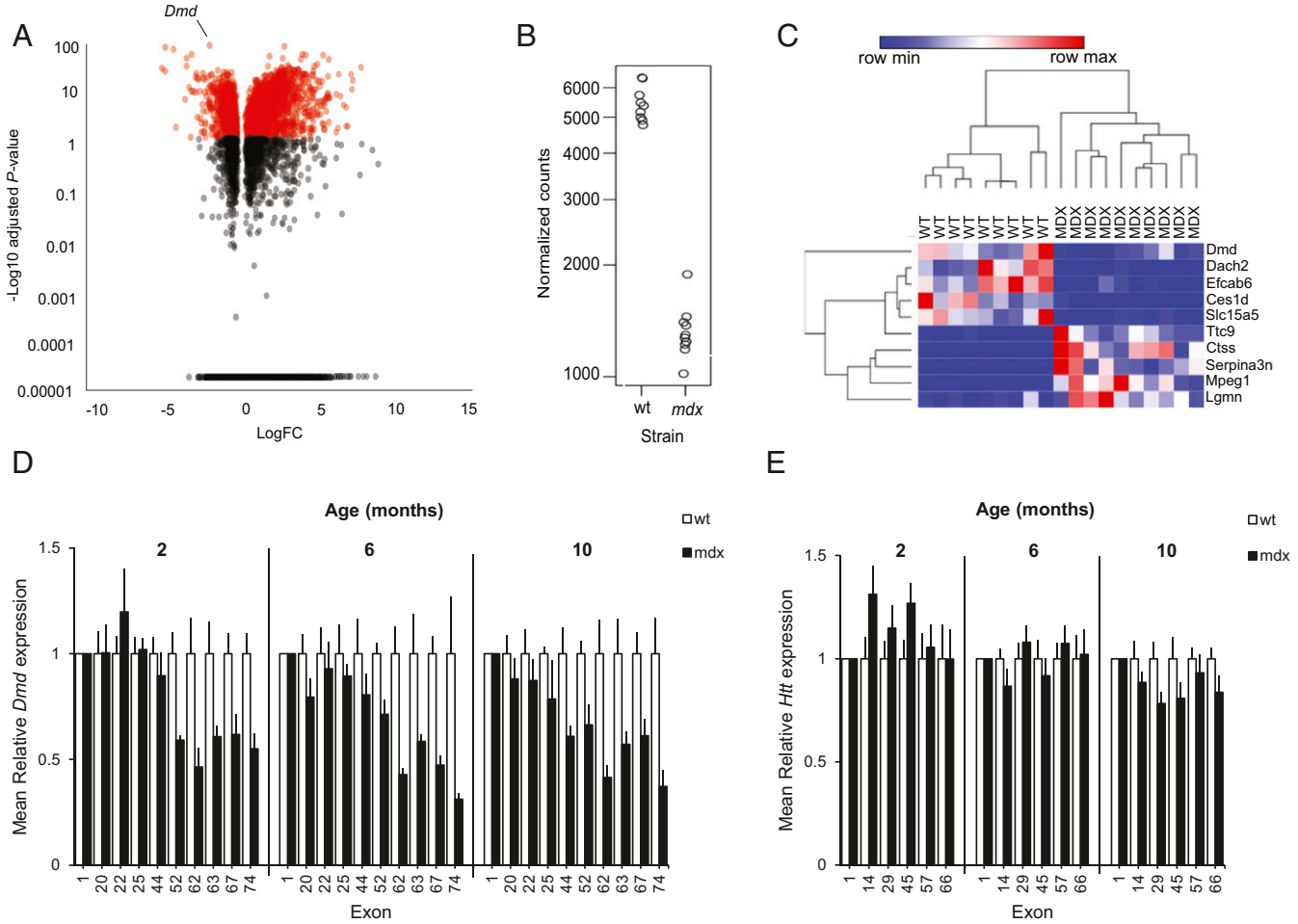

Fig. 1. The Dmd transcript is reduced in *mdx* mice compared to wt mice. (*A*) Volcano plot showing differentially expression analysis of RNA-seq data obtained from 9 wt and 10 *mdx* mice tibialis anterior muscles. Mice were 30 wk old. The *Dmd* gene is pointed by a line. The *x* axis shows the log2 fold change, while the *y* axis shows the −log10 of the Bonferroni-corrected *P* value. (*B*) Dot plot showing reduced normalized counts mapping to the *Dmd* gene in *mdx* mice compared to wt mice. (*C*) Heatmap showing complete clustering of wt and *mdx* mice based on the top 10 differentially expressed genes. (*D*) Bar chart showing relative expression levels obtained for several dystrophin exon−exon junctions along the *Dmd* gene in *mdx* and wt mice at 2, 6, and 10 mo of age (*N* is eight or nine mice per group). The exons mentioned on the *x* axis represent the location of the forward primer. Reduction of Dmd transcript toward the 3′ end compared to the wt counterpart was observed in all age groups. Error bars represent SE. (*E*) Bar chart showing relative expression levels obtained for exon−exon junctions along the *Htt* gene in *mdx* and wt mice at 2, 6, and 10 mo of age. Error bars represent SE.

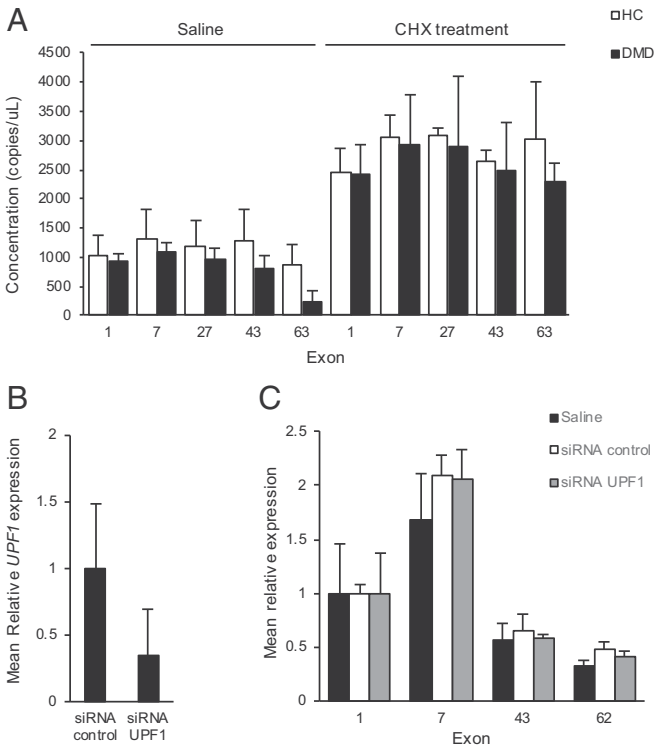

Fig. 2. Inhibition of NMD does not correct DMD transcript instability showed in DMD-derived myotubes compared to HCs. (*A*) Absolute transcript quantification performed by ddPCR is plotted on the *y* axis, while exons are plotted on the *x* axis representing the location of the forward primer. Bar chart shows the distribution of DMD transcripts obtained for several dystrophin exon–exon junctions in DMD (deletion of exons 48 to 50) cells compared to HCs treated with CHX (*Right*) or untreated (*Left*). (*B*) Bar graph shows the expression of *UPF1* gene when both control siRNA and siRNA targeting UPF1 were transfected in primary DMD-derived (point mutation in exon 6) myotubes. (*C*) Bar graph shows the distribution of qPCR data obtained for different dystrophin exon–exon junctions in primary DMD-derived myotubes after siRNA down-regulation of UPF1. Data represented were normalized to exon 1. Exons plotted on the *x* axis represent the location of the forward primer. All error bars represent SE.

NMD is not responsible for the observed 3′ end degradation of the DMD transcript (Fig. 2*C*).

To understand whether a nuclear or cytoplasmic mechanism could be responsible for the observed reduction at the transcriptional level, we studied the localization of the Dmd mRNA in skeletal muscles. RNA in situ hybridization (ISH) was performed on muscle sections of wt mice with positive (probe *Polr2a*) and negative (bacterial probe DapB) control probes (Fig. 3 *A* and *B*). ISH with probes targeting the Dmd mRNA suggested preferential nuclear localization (Fig. 3*C*). Probe specificity was confirmed in 3T3 mouse fibroblasts, where the *Dmd* gene is not expressed (*SI Appendix*, Fig. S1). To confirm nuclear localization, colocalization experiments were performed using fluorescent probes. The nuclear noncoding RNA Malat1 was used as nuclear localization signal, while ribosomal probes were used for cytoplasmic localization. Colocalization with Malat1 confirmed the nuclear localization of the Dmd mRNA; there was no evident colocalization of the Dmd transcript with ribosomal RNA stained with probes recognizing the 28S ribosomal structural component (Fig. 3 *D*–*H*). Fluorescent ISH analysis for *Ttn*, another large muscle-specific gene responsible for hereditary myopathy and early onset cardiomyopathy, showed colocalization with DAPI and Malat1 mRNA, indicating that nuclear localization is not dystrophin specific (Fig. 3 *I*–*M*). Interestingly, not all nuclei showed positive Dmd and Ttn mRNA signals. Dmd mRNA localization did not change in *mdx* mice, indicating that nuclear localization in skeletal muscle fibers is not mutation specific. However, the signal from the Dmd transcript appears to be lower in *mdx* mice compared to wt mice, which is in line with the reduced *Dmd* expression in *mdx* mice (Fig. 3 *N* and *O*). Nuclear localization was not affected by reading frame-restoring exon 23 skipping with either 2′-*O*-methylphosphorothioate (PS49) or morpholino oligomer (PMO) (Fig. 3 *P* and *Q*). Confirmation of the preferential nuclear localization of both DMD and TTN transcript was obtained in cultured human HC myotubes. Absolute transcript quantification by ddPCR was performed in purified nuclear fractions and whole-cell extracts. The ratio of whole-cell:nuclear counts was below 1 for DMD, TTN, and MALAT1 transcripts, confirming their preferential nuclear localization. A higher ratio above 1 was observed for 18S ribosomal RNA, suggesting a more cytoplasmic localization (Fig. 3*R*). Most importantly, the nuclear localization of the DMD transcript supported an NMD-independent mechanism to be responsible for reduced DMD mRNA levels, as NMD surveillance is a cytoplasmic mechanism and DMD mRNA is primarily localized in the nuclei.

It has been described, in literature, that the *DMD* locus is transcriptionally challenging, given the reduced accumulation of transcript at the 3′ end in control muscle (20), the presence of RNA polymerase II pausing sites in the *DMD* introns (e.g., intron 52) (22), the presence of multiple intronic polyadenylated RNAs (23, 24) and a complex nonsequential splicing process (25). Gene expression studies performed so far provided information about the steady-state level of DMD mRNA. To specifically study pre-mRNA synthesis and decipher whether a transcriptional mechanism is responsible for the reduced accumulation levels at the 3′ end, we performed a run-on experiment based on metabolic labeling of nascent RNA. HC- and DMD-derived (deletion of exons 48 to 50) myotubes were treated for 30 min with bromouridine (Bru), a uridine derivative that can be incorporated into newly synthesized RNA. After total RNA isolation, labeled RNA was captured using magnetic beads conjugated with anti-BrdU antibodies according to a previously published protocol (26). Sequencing of labeled RNA (Bru-RNA) showed reduced transcriptional output in the *DMD* locus in DMD-derived cells compared to HCs, indicating that the *DMD* gene is less transcribed in the presence of PTC (Fig. 4*A*). The result was confirmed in an independent experiment, where Bru-RNA RT-qPCR analysis was carried out using multiple primer pairs along the *DMD* gene. Bru-RNA RT-qPCR data confirmed not only the reduced DMD transcript levels in DMD cells compared to HCs but also the observed reduction toward the 3′ end (Fig. 4*B*).

We hypothesized that reduced transcriptional output could be the result of the PTC leading to a chromatin conformation that is less prone to transcription. Chromatin immunoprecipitation (ChIP) was performed on tissue (quadriceps and gastrocnemii muscles) obtained from wt and *mdx* mice. Antibodies recognizing histone 3 (H3), H3 lysine 4 trimethylation (H3K4me3), H3 lysine 9 trimethylation (H3K9me3), H3 lysine 27 trimethylation (H3K27me3), H3 lysine 36 trimethylation (H3K36me3), and IgG were used. The *Gapdh* gene was analyzed as control gene undergoing active transcription, while the *Pkd2l1* gene was taken as inactive gene control. Analysis of qPCR data at the promoter site of the *Gapdh* gene showed enrichment of the H3K4me3 mark in exon 1, indicating a favorable chromatin conformation for transcription at this location, while, at exon 6 location, H3K36me3 was elevated, showing ongoing transcription, as expected for both *mdx* and wt mice (Fig. 5*A*). Analysis of the *Dmd* gene at several genomic regions was performed for each antibody independently. ChIP with H3K4me3 antibody showed a clear enrichment at the promoter site compared to the following exons ($P < 10^{-14}$) for

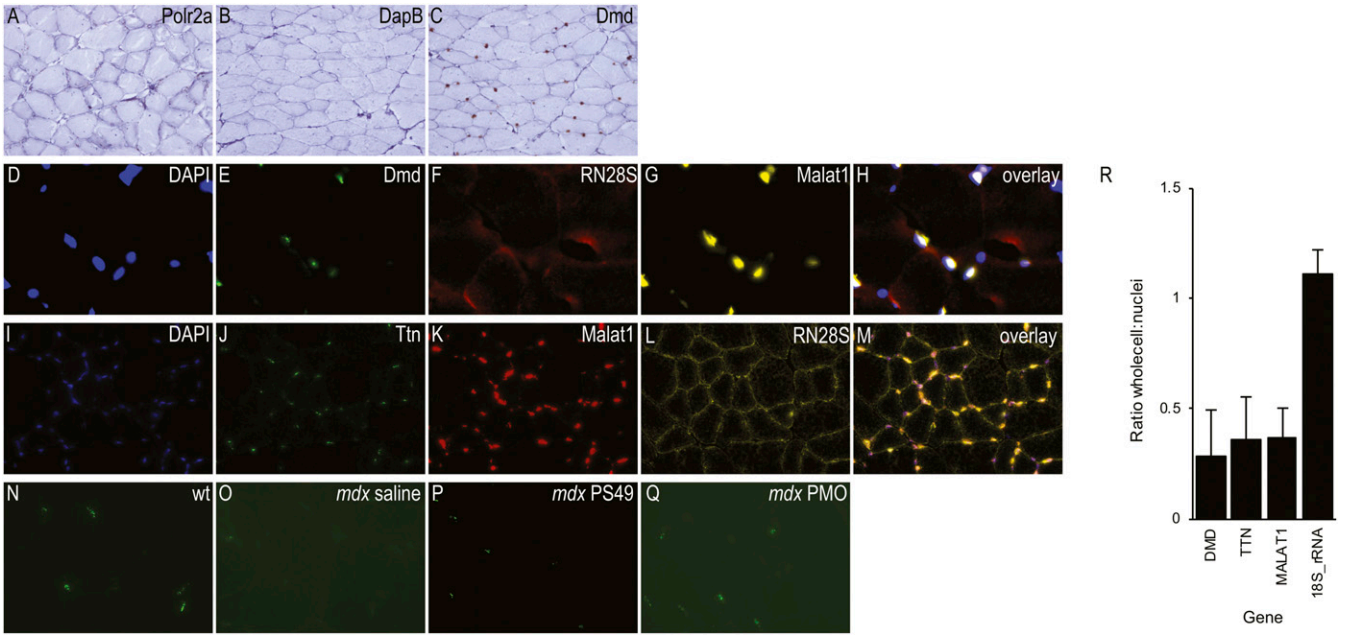

Fig. 3. ISH shows nuclear localization of the dystrophin mRNA in muscle. (*A–C*) Staining of tibialis anterior muscle of wt mice with single probes. The brown dots represent diaminobenzidine (DAB) signal obtained with the RNA Scope Brown assay for the positive control probe targeting (*A*) the Polr2a transcript, (*B*) the negative control bacterial dihydrodipicolinate reductase (DapB), and (*C*) Dmd mRNA. Images show a 20× magnification. (*D–H*) Multicolor staining using fluorescent probes to study Dmd mRNA localization. (*D*) DAPI, (*E*) Dmd, (*F*) RN28S, and (*G*) Malat1. Images show a 63× magnification. (*I–M*) Multicolor staining using fluorescent probes to study Ttn mRNA localization. (*I*) DAPI, (*J*) Ttn, (*K*) Malat1, and (*L*) RN28S. Images show a 40× magnification. *H* and *M* represent the overlay of the different channels. (*N–Q*) In situ RNA hybridization with Dmd specific probes in muscle from *mdx* mice untreated or treated with antisense oligonucleotides compared to wt. *N* represents staining in wt mice, *O* represents staining in *mdx* untreated mice, and *P* and *Q* show *mdx* mice treated with 2OMePS antisense oligonucleotides (in *P*) or morpholino antisense oligonucleotides (in *Q*). Images show a 63× magnification. (*R*) Bar graph shows the ratio of whole-cell:nuclear counts of DMD, TTN, MALAT1, and 18S ribosomal RNA transcripts. Absolute quantification of nuclear and whole-cell counts was performed by ddPCR in HC myotubes. Error bars represent SE.

both *mdx* and wt mice, indicating a chromatin conformation prone to transcription initiation. Presence of H3K36me3 was comparable across the gene between *mdx* and wt mice, with an increase visible at exon 76 ($P = 0.018$), indicating ongoing transcription of the most distal isoform Dp71. Immunoprecipitation with H3K9me3 showed an increased signal in *mdx* mice compared to wt ($P = 0.003$), indicating a more closed chromatin conformation in *mdx* compared to wt. H3K27me3 levels across the gene were in the range of the background signal and comparable to IgG levels in both wt and *mdx* mice. For this reason, no statistics were performed on H3K27me3. Although higher levels of H3 were observed in wt mice compared to *mdx* mice, no significant difference was found (Fig. 5*B* and *SI Appendix*, Fig. S2). To assess the differences at each exon site, we included the interaction between exon and group (wt and *mdx* mice) in the model, but no significant interaction was detected. Analysis of the *Pkd2l1* gene showed histone marks compatible with repressed transcription in both wt and *mdx* mice (Fig. 5*C*). Consistently with the immunoprecipitation results, higher levels of H3K9me3 were observed in *mdx* quadriceps muscle compared to wt by Western blot (WB) (Fig. 5*D*). Moreover, RNA-seq data showed increased expression of histone methyltransferases (HMTs) *Suv39h1* and *Setdb1* genes in *mdx* mice compared to wt mice, which are responsible for Lys-9 trimethylation of H3, and which play a vital role in heterochromatin organization. The expression of HMTs responsible for H3K36 trimethylation such as Nsd1 and Setd2 was not affected in *mdx* mice compared to wt (Fig. 5*E*). Considering that H3K9me3, one of the specific tags for transcriptional repression, and H3K9me3-responsible HMTs are highly expressed in *mdx* mice compared to wt, we reasoned that an epigenetic mechanism could be involved in the reduced DMD transcript levels observed in the presence of PTC.

Recent studies performed in mouse models of muscular dystrophy have demonstrated that histone deacetylase inhibitor(s) (HDACi) counter the progression of the disease (27). HDACi are known to improve regeneration in dystrophic muscles by promoting myogenesis through follistatin up-regulation (28). Givinostat is an HDACi, which is currently being evaluated in a phase 3 placebo-controlled clinical trial in DMD patients. Givinostat is an HDACi that inhibits histone deacetylation, leading to active gene transcription. To assess whether givinostat is able to counteract the transcriptional repression observed in the presence of a PTC, *mdx* mice were treated with different doses of givinostat (5 mg/kg and 10 mg/kg) for 14 wk. RT-qPCR data obtained from diaphragm muscle after treatment showed a significant increase of *DMD* expression in mice treated with different givinostat doses compared to mice treated with placebo (methylcellulose [MC]) ($P = 0.001$). In particular, givinostat treatment had a larger effect on first exons (~20% increase of *DMD* expression) compared to exons toward the 3′ end ($P = 0.005$) (Fig. 5*F*). Although the epigenetic mechanism leading to the observations remains to be elucidated, these results support our hypothesis, according to which, epigenetic changes are responsible for the reduced dystrophin levels observed in the presence of PTC.

Discussion

DMD and BMD are caused by mutations in the *DMD* gene (29). DMD patients experience a more severe disease course compared to BMD patients, with reduced life expectancy and inability to walk beginning from the age of 10 y to 12 y (30). BMD patients, conversely, experience a more variable but generally milder disease course, with normal life expectancy. At the genetic level, the difference between DMD and BMD individuals is

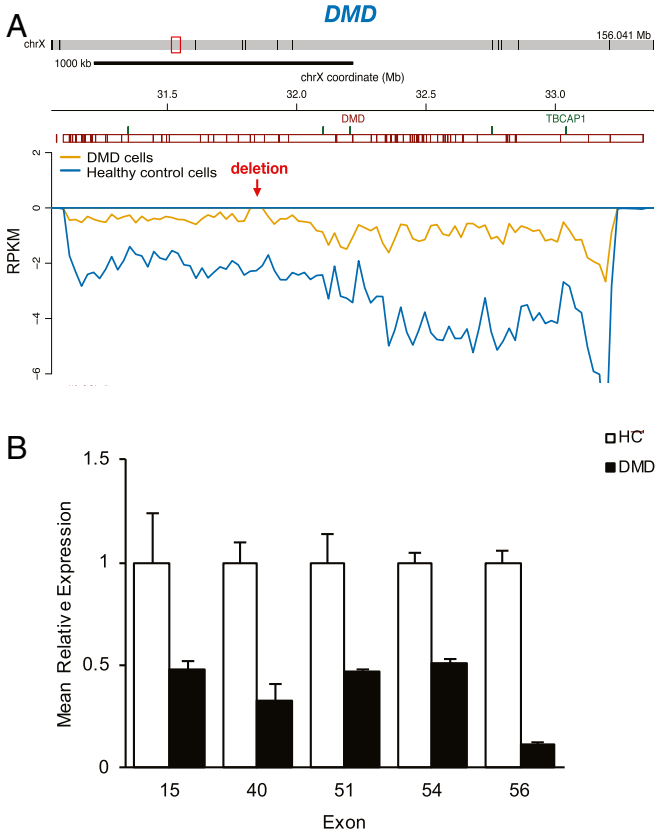

Fig. 4. The rate of DMD transcription is lower in DMD cells compared to HCs. (*A*) Genome browser view showing a reduced amount of normalized read counts mapping to the *DMD* locus in DMD-derived cells compared to HC cells. Transcription reads are plotted below 0 because the *DMD* gene is transcribed from the negative strand. (*B*) Bar graph showing the distribution of Bru-RNA RT-qPCR data obtained for multiple primer pairs along the *DMD* gene in DMD cells and HCs. Error bars represent SE.

the presence or absence of PTC in the dystrophin mRNA coding sequence (31). DMD patients have mRNAs with premature stop codons resulting in complete absence of dystrophin, while BMD patients present mRNAs without stop codons that are longer or shorter and encode partially functional dystrophin proteins. Multiple therapeutic approaches aiming to convert DMD-causing mutations into BMD mutations at the RNA level have been developed and tested in DMD patients, including stop codon read-through (32) and exon skipping (33). These approaches received conditional and accelerated marketing authorizations by European Medicines Agency and Food and Drug Administration, respectively, and confirmatory trials are ongoing. Both therapeutic strategies target dystrophin transcripts. However, while the stop codon read-through application targets the mature cytoplasmic mRNAs, the exon-skipping strategy affects the nuclear processing of the transcript by inducing skipping of exons during pre-mRNA splicing. It has been widely reported that the drug target, namely the dystrophin transcript, is reduced in both DMD and BMD patients (10, 17). It has also been shown that the reduction is more prevalent at the 3′ end of the transcript in dystrophic mice and patients compared to wt mice and HCs (18, 19). While dystrophin mRNA reduction in DMD patients and *mdx* mice could be due to the cytoplasmic NMD mechanism, this is less likely for BMD patients, where premature stop codons are not present, even though it has been reported that normally occurring transcripts can still be substrates of NMD (34).

In this study, we show that the dystrophin transcript localizes primarily in the nuclear compartment of muscle fibers in vivo in both healthy and dystrophic conditions. The nuclear localization is not affected by treatment with antisense oligonucleotides (both 2*O*MePS and PMO) known to affect splicing and restore the reading frame. The finding that the dystrophin mRNA localizes in the nuclei supports the notion that NMD inhibition does not result in restoration of the reduced 3′ end transcript levels observed in DMD. Treatment with CHX (a translation inhibitor and therefore NMD inhibitor) was, however, responsible for an overall increase of dystrophin transcript in both healthy and DMD-derived muscle cell cultures, showing that the dystrophin mRNA is targeted by NMD in cultured cells even in the absence of premature stop codons. Dystrophin mRNA degradation by means of NMD surveillance is proven to be inefficient in vivo, as dystrophin mRNA is routinely purified and analyzed from muscle biopsies of DMD patients for diagnostic purposes (35, 36); this is particularly true for the more distal mutations, as it has been reported that mutations downstream of exon 70 can evade NMD (37). The overall efficacy of NMD in skeletal muscle is unclear, as RNA-based diagnostic protocols from muscle biopsies are widely used for neuromuscular disorders beyond DMD. It has been occasionally reported that nonsense or frameshifting mutations lead to a drastic reduction of transcript levels, as in patients with limb girdle muscular dystrophy type 2A carrying mutations in the *CAPN3* gene (38). However, nonsense mutations on both alleles of the *PYGM* gene can still lead to high transcript levels up to 40% (39). Virtually all NMD evidence in the muscle field has been collected in cultured cells (40). Here we show that large transcripts such as dystrophin and titin are preferentially located in the nuclear compartment, suggesting that NMD is not the primary mechanism responsible for reduced dystrophin mRNA levels. This observation is consistent with recent RNAscope data deposited in bioRxiv, showing that nascent dystrophin transcripts are reduced within the nuclei in dystrophic muscles compared to healthy muscles and suggesting that transcription degradation via NMD is not responsible for the reduction observed (41).

To elucidate whether a nuclear mechanism could be responsible for the reduced dystrophin transcript levels at the 3′ end, we studied RNA synthesis rate in HC- and DMD-derived cells. Labeling of nascent RNA with Bru followed by Bru capture and sequencing revealed a reduced transcriptional output at the *DMD* locus in the presence of PTC, suggesting a transcriptional mechanism involved in the reduction observed. Considering that production of RNA is mainly regulated by epigenetic marks, we studied the chromatin conformation of the *Dmd* locus in *mdx* and wt mice muscles to understand whether the presence of PTC could affect the accessibility of chromatin to the transcription machinery in vivo. The collected data after ChIP showed increased H3K9me3 modification in *mdx* compared to wt along the *Dmd* locus; this observation suggests a chromatin conformation less prone to transcription in *mdx* mice compared to wt mice, explaining the reduced transcript accumulation toward the 3′ end.

H3K9 methylation is a transcriptionally repressive mark that competes with the transcriptional permissive H3K9 acetylation (42). Hence, promoting H3K9 acetylation should counteract the effects of increased H3K9 methylation observed in the presence of PTC. To assess whether increased histone acetylation (and therefore decreased histone methylation) could recover dystrophin levels, we treated *mdx* mice with the HDACi givinostat. Analysis of RNA by RT-qPCR showed an increase in *DMD* expression (~20%) after treatment with two different givinostat doses (5 mg/kg and 10 mg/kg). Previous studies demonstrated that HDACs interact physically with SUV39H1 (43), one of the methyltransferases responsible for H3K9me3 methylation whose increased expression in *mdx* mice compared to wt mice explains

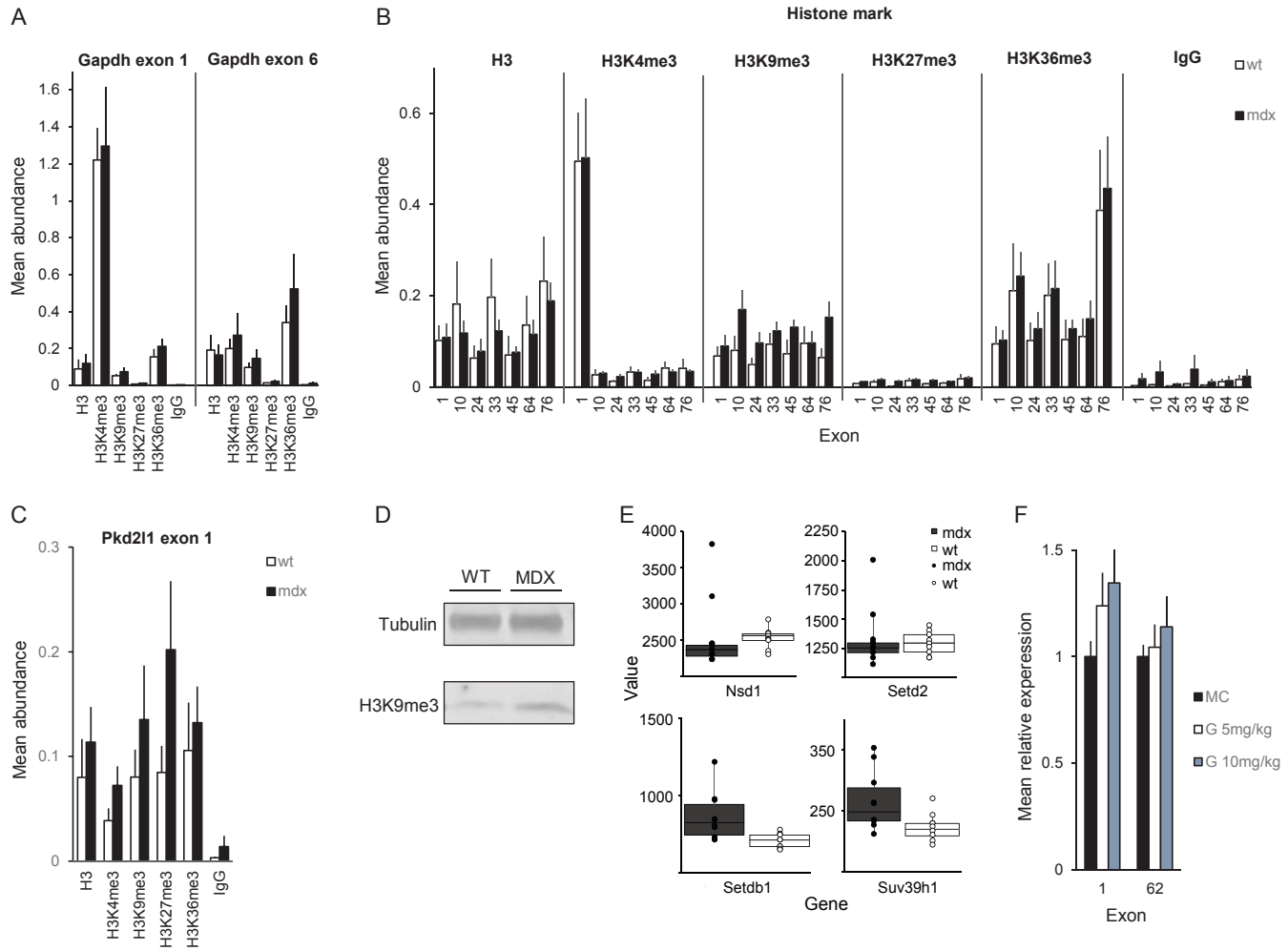

Fig. 5. Epigenetic changes identified in *mdx* mice compared to wt mice. (*A*–*C*) ChIP qPCR data of wt and *mdx* quadriceps muscles. *N* is five mice per group. (*A*) Bar graph showing the mean abundance of amplified DNA for exon 1 (*Left*) and exon 6 (*Right*) of the *Gapdh* gene for H3, H3k4me3, H3k9me3, H3K27me3, H3K36me3, and IgG. (*B*) Bar graph showing the mean abundance of amplified DNA across the *Dmd* locus. Histone marks are reported on top of each panel. (*C*) Bar graph showing the mean abundance of amplified DNA for exon 1 of the *Pk2dl1* gene. Error bars in *A*–*C* represent SE. (*D*) Western blotting analysis of H3K9me3 expression in *mdx* mice compared to wt mice. Tubulin expression is used as loading control. (*E*) Box plot showing increased normalized counts mapping to the *Suv39h1* and *Setdb1* genes in *mdx* mice compared to wt mice. No significant difference is observed in the expression of *Nsd1* and *Setd2* genes between *mdx* and wt mice. (*F*) Bar graph showing relative *Dmd* expression in *mdx* mice treated either with placebo (MC) or two different doses of the HDACi givinostat (G) (5 mg/kg and 10 mg/kg). Quantification was performed by qPCR targeting exons 1 and 2 and exons 62 to 64 junctions of the *Dmd* gene.

the higher levels of H3K9me3 observed by WB. Most importantly, other HMTs were not differentially expressed between *mdx* and wt mice, suggesting a transcriptional repressive mechanism responsible for the reduced dystrophin mRNA levels observed. HDACs and SUV39H1 constitute a complex involved in heterochromatin silencing where histone deacetylases are required for the Lys-9 deacetylation followed by methylation by SUV39H1 resulting in transcriptional repression (44) (Fig. 6*A*). In the presence of HDACi, transcriptional repression by SUV39H1 is mostly abolished (43), suggesting a possible mechanism where HDACi such as givinostat are able to keep Lys-9 acetylated, avoiding its methylation by SUV39H1 and therefore recovering dystrophin expression levels (Fig. 6*B*).

The data presented in this report support the hypothesis that transcriptional dynamics across the *DMD* locus are affected by the presence of PTC and that this process is likely mediated by histone marks. This report shows preferential nuclear localization of the mRNA in muscle tissue, and it observes that PTC can cause regional changes in transcriptional dynamics.

Materials and Methods

Animal Procedures. The wt and *mdx* mice carrying a nonsense mutation in exon 23 of the *Dmd* gene were included in the experiment. Dmd and Htt transcript quantification by qPCR was performed on muscles obtained from mice involved in a previously published paper (45). RNA-seq analysis was performed on tibialis anterior muscles of 30-wk-old mice. A total of 9 wt and 10 *mdx* mice were used. ChIP analysis was performed on quadriceps and gastrocnemii muscles of 30-wk-old mice. A total of 20 muscles were analyzed; specifically, 10 quadriceps (5 wt and 5 *mdx*) and 10 gastrocnemii (5 wt and 5 *mdx*) were included. ISH was performed on tissue sections of 8 μm obtained from tibialis anterior muscle of 30-wk-old wt and *mdx* mice. Further staining was performed on muscles obtained from mice treated with antisense oligonucleotides. Mice received either 100 mg/kg/wk of PMO or 200 mg/kg/wk of 2OMePS AON by intravenous injection in the tail vein. Treatment started at 6 wk of age, and mice were treated for eight consecutive weeks. One week after the last injection, animals were killed by cervical dislocation. Tissues were frozen in liquid nitrogen-cooled isopethane. *Mdx* mice were treated with the HDACi givinostat (Italfarmaco) for 14 wk starting at 4 to 5 wk old. They received either MC or different doses of givinostat (5 mg/kg or 10 mg/kg) by oral gavage five times per week. A total of five mice per group were used. The experiments were evaluated and

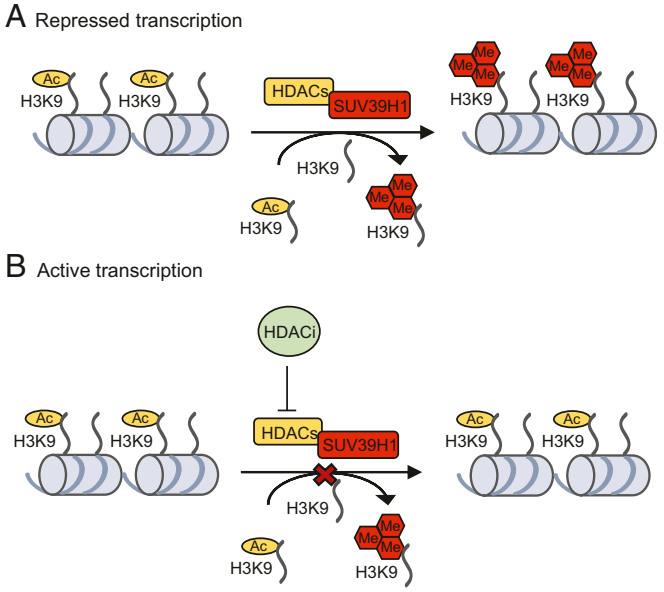

Fig. 6. Schematic representation of the proposed molecular model responsible for reduced DMD mRNA levels in the presence of PTC. *A* represents the hypothesized mechanism responsible for the repressed *DMD* transcription observed. HDACs–SUV39H1 complex is involved in heterochromatin silencing where HDACs are required for the Lys-9 deacetylation of H3 to allow its methylation by SUV39H1. Increased levels of H3K9me3 lead to a chromatin conformation less prone to transcription and, therefore, to reduced DMD mRNA levels. *B* represents how HDACi such as givinostat could counteract the repressed *DMD* transcription observed. When HDACi are present, HDACs cannot deacetylate Lys-9 of H3, and it remains acetylated, avoiding its methylation by SUV39H1. Increased histone acetylation leads to a chromatin conformation prone to transcription and, therefore, to a possible recovery of DMD mRNA levels.

approved by the local animal welfare committee under DEC numbers 13154 and AVD1160020171407.

RNA Analysis. Total RNA was purified using TriPure isolation reagent (Sigma) following manufacturer's protocol. Oligo dT-based library preparation was performed using the Illumina Truseq kit by Illumina. Paired-end sequencing was performed on the Illumina HiSeq 2500. For qPCR analysis, 400 ng of total RNA was used for complementary DNA (cDNA) synthesis using random hexamers and the Transcriptor kit (Roche). The qPCR was performed on the LC480 Light Cycler (Roche) using SYBR Green intercalating dye (SensiMix, Bioline). All primer pairs used in qPCR spanned at least one splice junction.

Cell Culture. HC (KM155) and DMD (8036, deletion of exons 48 to 50) immortalized myoblasts were plated on 0.5% gelatin coated six-well plates. A total of 300,000 cells per well were plated. Cells were induced to differentiate to myotubes 24 h after plating, according to a previously described protocol (46). After 3 d of differentiation, cells were either treated with 100 μM CHX or saline solution. Each condition was tested in three replicates. RNA isolation was performed with TriPure isolation reagent (Sigma) 24 h after treatment. For ddPCR analysis, 500 ng of total RNA was used. The ddPCR (Bio-Rad) was performed using EVA Green as intercalating dye. Droplets were generated with the QX200 system (catalog no. 1864100, Bio-Rad) using cartridges (catalog no. 1864108, Bio-Rad). The droplet QX200 reader (catalog no. 1864100, Bio-Rad) was used to count positive and negative droplets.

Primary DMD-derived (41/03, point mutation in exon 6) myoblasts obtained by Eurobiobank were plated on 0.5% gelatin coated 12-well plates. A total of 40,000 cells per well were plated. When cells were confluent, they were induced to differentiate to myotubes. After 1 d of differentiation, cells were transfected with both siRNA control and siRNA directed against UPF1 transcript at a final concentration of 100 nM. Each condition was tested in three replicates. RNA isolation using TriPure isolation reagent (Sigma) was performed 48 h after transfection. For further RT-qPCR analysis, 400 ng of total RNA was used.

To purify the nuclei fraction, cells were washed and trypsinized, followed by centrifugation (10 min, 1,200 rpm). Ice-cold nuclear isolation buffer (10 mM Tris·HCl pH 7.5, 10 mM NaCl, 3 mM $MgCl_2$, RNase inhibitor) and lysis buffer (nuclear isolation buffer with 1% IGEPAL CA-630) were added. After mixing by pipetting, the lysate was transferred onto a 20-μm filter to remove cytoplasmic proteins and cell debris. The flowthrough containing the isolated nuclei was centrifuged 5 min at 4 °C and 500 relative centrifugal force. The nuclei pellet was resuspended in TriPure for RNA isolation. For ddPCR analysis, 100 ng of total RNA was used.

ISH. ISH was performed using RNAscope 2.5 HD Reagent Kit brown and the RNAscope Fluorescent Multiplex Reagent Kit (ACD BIO). Mm-polar2a (catalog no. 312471) was used as positive control probe, while DapB (catalog no. 310043) was used as negative probe for the brown kit. RNAscope 3-plex Positive Control Probe (catalog no. 320881) and RNAscope 3-plex Negative Control Probe (catalog no. 320871) were used with the fluorescent kit. Two independent probes targeting the Dmd transcript were used: probe with catalog no. 411201 contains five Z pairs and targets the region between nucleotides 21 and 307, while probe with catalog no. 452801 has 20 Z pairs and targets the region between nucleotides 320 and 1,295 mapped on National Center for Biotechnology Information Reference Sequence NM_007868.5. Other probes used were Mm-Ttn (catalog no. 483031), Mm-Malat1 (catalog no. 313391), and Mm-Rn28s1 (catalog no. 502281).

Bru Labeling and Isolation of Bru-RNA. HC (KM155) and DMD (8036, deletion of exons 48 to 50) immortalized myoblasts were plated on 0.5% gelatin-coated Petri dishes (Ø = 15 cm) for Bru-RNA RT-qPCR analysis and on 0.5% gelatin-coated Nunclon Petri dishes (245 mm × 245 mm × 20 mm) for Bru-RNA sequencing. Once the cells were 90% confluent, they were rinsed once with Hanks' balanced salt solution (HBSS) and induced to differentiate to myotubes. After 3 d of differentiation, Bru (Sigma) was added to the medium at a final concentration of 2 mM, and cells were incubated at 37 °C for 30 min to label nascent RNA. Cells were then washed twice with HBSS and collected directly. Total RNA was isolated using TriPure reagent (Sigma), and Bru-RNA was immunopurified from total RNA using anti-BrdU antibodies (BD Biosciences) conjugated to magnetic beads (Dynabeads, Goat anti-Mouse IgG; Invitrogen) under gentle agitation for 1 h at room temperature. For more details, the procedure was performed according to a previously described protocol (26).

cDNA Library Preparation and Illumina Sequencing of Bru-RNA. Isolated Bru-RNA was used to prepare cDNA libraries using the Illumina TruSeq Kit (Illumina). Sequencing of the cDNA libraries prepared from nascent RNA and further analysis was done in collaboration with the research group of Mats Ljungman at the University of Michigan Sequencing Core. Illumina HiSeq 2000 sequencer was used for the sequencing.

Bru-RNA RT-qPCR Quantification. For qPCR analysis, 90 ng of isolated Bru-RNA were used for cDNA synthesis using random hexamers and BioScript Reverse Transcriptase (Bioline). The qPCR was performed on the LC480 Light Cycler (Roche) using SYBR Green (SensiMix, Bioline) as intercalating dye. Multiple primer pairs were used along the *Dmd* gene. Forward and reverse primers were used within the same exon, since the dystrophin transcript contains long introns (24 over 10 kb long and 5 over 100 kb long) that may not be removed during the 30 min of Bru labeling.

ChIP. Quadriceps and gastrocnemii of mice were collected and frozen in liquid nitrogen. Analysis was performed according to a previously published protocol (47). Briefly, about 150 mg of frozen tissue was used to prepare chromatin. Tissue was ground into powder using an ice-cold mortar. Before cross-linking, samples were vortexed and incubated in relaxation buffer containing 10 mM KCl, 5 mM MgCl2 · 6 H_2O, 5 mM EGTA (pH 8), 5 mM Tetrasodium pyrophosphate, 1 mM phenylmethylsulfonyl fluoride (PMSF), and 1× Protease inhibitors for 30 min on ice. Samples were then centrifugated, and pellets were resuspended in phosphate-buffered saline (PBS) containing 1% formaldehyde. Cross-linking was performed for 10 min at room temperature under agitation (800 rpm) and quenched in 125 mM of glycine for 5 min at room temperature. Samples were then washed twice in ice-cold PBS before incubation in lysis buffer containing 10 mM Tris·HCl (pH 8), 5 mM (ethylenedinitrilo)tetraacetic acid (EDTA) (pH 8), 85 mM KCl, 0.5% Nonidet P-40, 1 mM PMSF, and 1× Protease inhibitors for 10 min on ice. Homogenization was performed on the MagnaLyzer (Roche) using 1.4-mm zirconium beads tubes (Ops Diagnostics) for 30 s at 5,000 rpm. The homogenized material was collected and incubated twice in lysis buffer for 5 min on ice. After centrifugation, pellets were resuspended in a buffer

containing 150 mM NaCl, 50 mM Tris·HCl (pH 7.5), 5 mM EDTA (pH 8), 0.5% Nonidet P-40, 1% Triton X-100 before sonication in 1.5 mL of sonication tube (Diagenode) using the Bioruptor instrument (Diagenode) for 25 cycles. The samples were centrifuged to obtain a cleaned chromatin solution and were then loaded and visualized on agarose gel to assess whether sonication was successful. To estimate the amount of chromatin, DNA was purified from a fraction of the material using phenol-chloroform-isoamylalcohol (Invitrogen, ratio 25:24:1). DNA quantification was performed with the Nanodrop spectrophotometer (Isogen Life Science).

ChIP was performed as previously described (48, 49), using antibodies for H3 (ab1791, Abcam), H3K4me3 (17-614, Merck), H3K9me3 (39161, Actif Motif), H3K27me3 (17-622, Millipore), H3K36me3 (C15410058, Diagenode), and IgG (Sc-2025, Santa Cruz). Immunopurified DNA was analyzed by qPCR using SYBR Green as intercalating dye (SensiMix, Bioline). Prior to analysis, data were corrected for input DNA.

WB. WB was performed on quadriceps protein extracts after lysis in radioimmunoprecipitation assay buffer (20 mM Tris·HCl pH 7.5, 150 mM NaCl, 0.1% sodium dodecyl sulfate, 1% Nonidet P-40, 5 mM EDTA and 0.5% sodium deoxycholate), adding protease inhibitor mix. Then 50 μg of protein was resolved in a 4 to 20% Mini-PROTEAN TGX precast gel (Bio-Rad) and transferred onto nitrocellulose membrane at 25 V for 30 min (TransBlot Turbo Minisize Nitrocellulose membrane using the TransBlot Turbo System, BioRad). Unspecific binding was blocked for 1 h in 5% milk/PBS. Primary antibody incubation was performed overnight at 4 °C using the following antibodies: rabbit anti-H3K9me3 (Abcam, 1:1,000 in 1% milk/PBS) and mouse anti-tubulin (Sigma-Aldrich, 1:2,000 in 1% milk/PBS) as a loading control. Secondary antibody incubation was carried out for 1 h at 4 °C using goat anti-mouse IRDye800 (1:10,000 in 1% milk/PBS) and goat anti-rabbit IRDye680 (1:10,000 in 1% milk/PBS). Odyssey CLx (LICOR) using Image Studio Lite Software was used for the imaging.

Statistical Analysis. Alignment of fastq files to the *Mus musculus* genome assembly GRCm38 (mm10) was performed using the Spliced Transcripts Alignment to a Reference software (50). Analysis of count data was performed using the Deseq2 package. A Bonferroni correction for multiple testing was performed to identify differentially expressed genes between wt and *mdx* mice. Analysis of qPCR data was performed using the LinReg software to correct for differences in primer amplification efficiency (51). Data were normalized for *Gapdh* as housekeeping gene. Differences in gene expression along the *Dmd* gene were tested using a linear mixed model, where exon, group, and the interaction between gender and exon were included as fixed effects. Individual subjects were used as random effects, allowing random intercept. Analysis of ChIP qPCR data was performed for each antibody independently. H3K27me3 levels were not tested, as they were too close to IgG background. We used a linear model where exon, muscle, and group were included as factors. Only main effects were included in the model. Analysis of givinostat treatment was performed using a linear model where exon, treatment, and the interaction between treatment and exon were included as factors.

Data Availability. The RNA-seq data reported have been deposited in the Gene Expression Omnibus (GEO) database, https://www.ncbi.nlm.nih.gov/geo under accession number GSE132741. Bru-seq data is available under accession number GSE153453.

ACKNOWLEDGMENTS. We would like to acknowledge Laura van Vliet-van den Dool for the help with the ISH, and members of Mats Ljungman's laboratory for performing the sequencing of nascent Bru-labeled RNA and subsequent analysis. We thank the pharmaceutical company Italfarmaco for providing the HDACi givinostat, Dr. Vincent Mouly (Institute of Myology, Paris, France), and Muscle Tissue Culture Collection (MTCC) for providing the samples. MTCC is part of the German network on muscular dystrophies (MD-NET, Service Structure S1, Grant 01GM0601) and the German network for mitochondrial disorders (mito-NET, Project D2, Grant 01GM0862) funded by the German Ministry of Education and Research (Bonn, Germany). MTCC is a partner of EuroBioBank (http://www.eurobiobank.org/) and Treat Neuro-Muscular Disease network (https://treat-nmd.org/). This work was supported by the Prinses Beatrix Spierfonds under Grant Agreement W.OR14-13.

1. E. Mercuri, F. Muntoni, Muscular dystrophies. *Lancet* **381**, 845–860 (2013).
2. N. M. Goemans *et al*., Systemic administration of PRO051 in Duchenne's muscular dystrophy. *N. Engl. J. Med.* **364**, 1513–1522 (2011).
3. Y. Y. Syed, Eteplirsen: First global approval. *Drugs* **76**, 1699–1704 (2016).
4. R. S. Finkel *et al*., Phase 2a study of ataluren-mediated dystrophin production in patients with nonsense mutation Duchenne muscular dystrophy. *PLoS One* **8**, e81302 (2013).
5. H. Heemskerk *et al*., Preclinical PK and PD studies on 2′-O-methyl-phosphorothioate RNA antisense oligonucleotides in the mdx mouse model. *Mol. Ther.* **18**, 1210–1217 (2010).
6. C. Betts *et al*., Pip6-PMO, A new generation of peptide-oligonucleotide conjugates with improved cardiac exon skipping activity for DMD treatment. *Mol. Ther. Nucleic Acids* **1**, e38 (2012).
7. A. Goyenvalle *et al*., Functional correction in mouse models of muscular dystrophy using exon-skipping tricyclo-DNA oligomers. *Nat. Med.* **21**, 270–275 (2015).
8. S. Cirak *et al*., Exon skipping and dystrophin restoration in patients with Duchenne muscular dystrophy after systemic phosphorodiamidate morpholino oligomer treatment: An open-label, phase 2, dose-escalation study. *Lancet* **378**, 595–605 (2011).
9. J. Chamberlain *et al*., Expression of the murine Duchenne muscular dystrophy gene in muscle and brain. *Science* **239**, 1416–1418 (1988).
10. J. N. Haslett *et al*., Gene expression comparison of biopsies from Duchenne muscular dystrophy (DMD) and normal skeletal muscle. *Proc. Natl. Acad. Sci. U.S.A.* **99**, 15000–15005 (2002).
11. R. S. Finkel, Read-through strategies for suppression of nonsense mutations in Duchenne/Becker muscular dystrophy: Aminoglycosides and ataluren (PTC124). *J. Child Neurol.* **25**, 1158–1164 (2010).
12. S. D. Wilton *et al*., Antisense oligonucleotide-induced exon skipping across the human dystrophin gene transcript. *Mol. Ther.* **15**, 1288–1296 (2007).
13. Y. Aoki, T. Yokota, M. J. Wood, Development of multiexon skipping antisense oligonucleotide therapy for Duchenne muscular dystrophy. *BioMed Res. Int.* **2013**, 402369 (2013).
14. M. Bremmer-Bout *et al*., Targeted exon skipping in transgenic hDMD mice: A model for direct preclinical screening of human-specific antisense oligonucleotides. *Mol. Ther.* **10**, 232–240 (2004).
15. N. H. Gehring *et al*., Exon-junction complex components specify distinct routes of nonsense-mediated mRNA decay with differential cofactor requirements. *Mol. Cell* **20**, 65–75 (2005).
16. S. Tuffery-Giraud *et al*., Mutation spectrum leading to an attenuated phenotype in dystrophinopathies. *Eur. J. Hum. Genet.* **13**, 1254–1260 (2005).
17. D. Nitsch *et al*., Network analysis of differential expression for the identification of disease-causing genes. *PLoS One* **4**, e5526 (2009).
18. P. Spitali *et al*., DMD transcript imbalance determines dystrophin levels. *FASEB J.* **27**, 4909–4916 (2013).
19. K. Anthony *et al*., Biochemical characterization of patients with in-frame or out-of-frame DMD deletions pertinent to exon 44 or 45 skipping. *JAMA Neurol.* **71**, 32–40 (2014).
20. C. N. Tennyson, Q. Shi, R. G. Worton, Stability of the human dystrophin transcript in muscle. *Nucleic Acids Res.* **24**, 3059–3064 (1996).
21. N. Hug, D. Longman, J. F. Cáceres, Mechanism and regulation of the nonsense-mediated decay pathway. *Nucleic Acids Res.* **44**, 1483–1495 (2016).
22. S. Gherardi *et al*., Transcriptional and epigenetic analyses of the DMD locus reveal novel cis-acting DNA elements that govern muscle dystrophin expression. *Biochim. Biophys. Acta. Gene Regul. Mech.* **1860**, 1138–1147 (2017).
23. P. Spitali *et al*., G.P.3.07 Intronic conserved non-coding sequences (CNSs) as a tool to detect non-coding RNAs (ncRNAs) and putative regulatory motifs within the dystrophin gene. *Neuromuscul. Disord.* **17**, 784 (2007).
24. M. Bovolenta *et al*., The DMD locus harbours multiple long non-coding RNAs which orchestrate and control transcription of muscle dystrophin mRNA isoforms. *PLoS One* **7**, e45328 (2012).
25. I. Gazzoli *et al*., Non-sequential and multi-step splicing of the dystrophin transcript. *RNA Biol.* **13**, 290–305 (2016).
26. M. T. Paulsen *et al*., Use of Bru-Seq and BruChase-Seq for genome-wide assessment of the synthesis and stability of RNA. *Methods* **67**, 45–54 (2014).
27. P. Bettica *et al*., Histological effects of givinostat in boys with Duchenne muscular dystrophy. *Neuromuscul. Disord.* **26**, 643–649 (2016).
28. G. C. Minetti *et al*., Functional and morphological recovery of dystrophic muscles in mice treated with deacetylase inhibitors. *Nat. Med.* **12**, 1147–1150 (2006).
29. J. K. Mah *et al*., A systematic review and meta-analysis on the epidemiology of Duchenne and Becker muscular dystrophy. *Neuromuscul. Disord.* **24**, 482–491 (2014).
30. J. C. van den Bergen *et al*., Clinical characterisation of Becker muscular dystrophy patients predicts favourable outcome in exon-skipping therapy. *J. Neurol. Neurosurg. Psychiatry* **85**, 92–98 (2014).
31. K. M. Flanigan *et al*.; United Dystrophinopathy Project Consortium, Nonsense mutation-associated Becker muscular dystrophy: Interplay between exon definition and splicing regulatory elements within the DMD gene. *Hum. Mutat.* **32**, 299–308 (2011).
32. M. Haas *et al*., European Medicines Agency review of ataluren for the treatment of ambulant patients aged 5 years and older with Duchenne muscular dystrophy resulting from a nonsense mutation in the dystrophin gene. *Neuromuscul. Disord.* **25**, 5–13 (2015).
33. K. R. Q. Lim *et al*., Eteplirsen in the treatment of Duchenne muscular dystrophy. *Drug Des. Dev. Ther.* **11**, 533–545 (2017).
34. Q. Feng, S. Jagannathan, R. K. Bradley, The RNA surveillance factor UPF1 represses myogenesis via its E3 ubiquitin ligase activity. *Mol. Cell* **67**, 239–251.e6 (2017).
35. S. Tuffery-Giraud *et al*., The role of muscle biopsy in analysis of the dystrophin gene in Duchenne muscular dystrophy: Experience of a national referral centre. *Neuromuscul. Disord.* **14**, 650–658 (2004).

36. F. Gualandi *et al*., Transcriptional behavior of DMD gene duplications in DMD/BMD males. *Hum. Mutat.* **30**, E310–E319 (2009).
37. T. P. Kerr, C. A. Sewry, S. A. Robb, R. G. Roberts, Long mutant dystrophins and variable phenotypes: Evasion of nonsense-mediated decay? *Hum. Genet.* **109**, 402–407 (2001).
38. K. Stehlíková *et al*., Quantitative analysis of CAPN3 transcripts in LGMD2A patients: Involvement of nonsense-mediated mRNA decay. **17**, 143–147 (2007).
39. G. Nogales-Gadea *et al*., Expression of the muscle glycogen phosphorylase gene in patients with McArdle disease: The role of nonsense-mediated mRNA decay. *Hum. Mutat.* **29**, 277–283 (2008).
40. Q. Feng *et al*., A feedback loop between nonsense-mediated decay and the retrogene DUX4 in facioscapulohumeral muscular dystrophy. *eLife* **4**, e04996 (2015).
41. J. C. W. Hildyard *et al*., Multiplex in situ hybridization within a single transcript: RNA-scope reveals dystrophin mRNA dynamics. bioRxiv:10.1101/791780 (3 October 2019).
42. S. S. Ghare *et al*., Coordinated histone H3 methylation and acetylation regulate physiologic and pathologic fas ligand gene expression in human CD4+ T cells. *J. Immunol.* **193**, 412–421 (2014).
43. O. Vaute, E. Nicolas, L. Vandel, D. Trouche, Functional and physical interaction between the histone methyl transferase Suv39H1 and histone deacetylases. *Nucleic Acids Res.* **30**, 475–481 (2002).
44. S. Rea *et al*., Regulation of chromatin structure by site-specific histone H3 methyltransferases. *Nature* **406**, 593–599 (2000).
45. M. van Putten *et al*., Low dystrophin levels in heart can delay heart failure in mdx mice. *J. Mol. Cell. Cardiol.* **69**, 17–23 (2014).
46. M. Hiller *et al*., A multicenter comparison of quantification methods for antisense oligonucleotide-induced DMD exon 51 skipping in Duchenne muscular dystrophy cell cultures. *PLoS One* **13**, e0204485 (2018).
47. S.-A. David *et al*., An assessment of fixed and native chromatin preparation methods to study histone post-translational modifications at a whole genome scale in skeletal muscle tissue. *Biol. Proced. Online* **19**, 10 (2017).
48. J. Balog *et al*., Correlation analysis of clinical parameters with epigenetic modifications in the DUX4 promoter in FSHD. *Epigenetics* **7**, 579–584 (2012).
49. J. D. Nelson, O. Denisenko, K. Bomsztyk, Protocol for the fast chromatin immunoprecipitation (ChIP) method. *Nat. Protoc.* **1**, 179–185 (2006).
50. A. Dobin *et al*., STAR: Ultrafast universal RNA-seq aligner. *Bioinformatics* **29**, 15–21 (2013).
51. J. M. Ruijter *et al*., Amplification efficiency: Linking baseline and bias in the analysis of quantitative PCR data. *Nucleic Acids Res.* **37**, e45 (2009).